# A structural change in the kinesin motor protein that drives motility

**Sarah Rice*, Abel W. Lin†, Daniel Safer‡, Cynthia L. Hart§, Nariman Naber‖, Bridget O. Carragher¶, Shane M. Cain†, Elena Pechatnikova#, Elizabeth M. Wilson-Kubalek†, Michael Whittaker†, Edward Pate☆, Roger Cooke‖, Edwin W. Taylor#, Ronald A. Milligan† & Ronald D. Vale*§**

§ *The Howard Hughes Medical Institute, and the * Departments of Cellular and Molecular Pharmacology and ‖ Biochemistry and Biophysics, University of California, San Francisco, California 94143, USA*
† *Department of Cell Biology, The Scripps Research Institute, La Jolla, California 92037, USA*
‡ *Department of Physiology, University of Pennsylvania School of Medicine, Philadelphia, Pennsylvania 19104, USA*
¶ *Beckman Institute, Department of Cell and Structural Biology, University of Illinois at Urbana-Champaign, Urbana-Champaign, Illinois 61801, USA*
# *Department of Molecular Genetics and Cell Biology, University of Chicago, Chicago, Illinois 60637, USA*
☆ *Department of Pure and Applied Mathematics, Washington State University, Pullman, Washington 99164, USA*

**Kinesin motors power many motile processes by converting ATP energy into unidirectional motion along microtubules. The force-generating and enzymatic properties of conventional kinesin have been extensively studied; however, the structural basis of movement is unknown. Here we have detected and visualized a large conformational change of a ~15-amino-acid region (the neck linker) in kinesin using electron paramagnetic resonance, fluorescence resonance energy transfer, pre-steady state kinetics and cryo-electron microscopy. This region becomes immobilized and extended towards the microtubule 'plus' end when kinesin binds microtubules and ATP, and reverts to a more mobile conformation when γ-phosphate is released after nucleotide hydrolysis. This conformational change explains both the direction of kinesin motion and processive movement by the kinesin dimer.**

Microtubule-based motors of the kinesin superfamily are involved in intracellular transport, mitosis and meiosis, control of microtubule dynamics and signal transduction pathways[1]. To execute these various activities, different kinesin family members have distinct protein domains that confer unique cargo binding, regulatory and oligomerization properties. However, all kinesins have a homologous ~330-amino-acid 'catalytic core' that binds ATP and microtubules[2]. This catalytic core bears a striking structural similarity to the nucleotide-binding core of the actin-based motor myosin, suggesting that these two molecular motors originated from a common ancestor[3,4].

Conventional kinesin, a dimer of identical ~120K (120,000 relative molecular mass ($M_r$)) heavy chains that transports organelles towards the microtubule plus end, has served as an important model system for understanding biological motility. Conventional kinesin (hereafter called 'kinesin') is a highly processive motor that can take more than 100 consecutive 8-nm steps (the distance between two α/β subunits of tubulin) before dissociating[5,6]. Such processive motion requires coordination between the two motor domains in the kinesin dimer[7–9], and an alternating-site enzymatic mechanism has been proposed[10–12]. Although not processive, kinesin monomers produced by truncation also generate motility, provided that several monomers interact simultaneously with a microtubule[7–9].

Myosin-based movement is believed to be generated by the angular rotation of a long α-helix and its associated light chains that occurs after nucleotide hydrolysis and phosphate release[13–16]. However, kinesin lacks an elongated lever arm and thus may use another type of mechanical element. The 'neck linker', a ~15-amino-acid segment carboxy-terminal to the catalytic core (Fig. 1), has been suggested to be important for kinesin force generation, as its sequence is highly conserved among plus-end- but not minus-end-directed kinesin motors[2,17]. In support of this idea, analyses of protein chimaeras between opposite polarity motors in the kinesin superfamily implicate the neck region as a governor of directionality[17–19], and mutagenesis of the neck linker severely impairs motility while having relatively little effect on ATPase activity (R. Case and R.D.V., manuscript submitted). Cryo-electron microscopy (cryo-EM) studies have also found nucleotide-dependent conformational changes in the microtubule-bound kinesin dimer[20–22], which could potentially involve the neck linker. Here we have directly measured conformations of the kinesin neck linker in different nucleotide- and microtubule-binding states, and the results have allowed us to formulate a structural model for how kinesin moves along a microtubule.

## Generation of a cysteine-light kinesin

To measure structural changes, we engineered a human kinesin without solvent-exposed cysteines, which has normal enzymatic and motile properties (see Methods). We introduced cysteines at defined locations for the attachment of biophysical probes. Cysteine 333 was chosen as a primary site, because its location is ideal for detecting potential motions of the neck linker relative to the catalytic core. Modification of this cysteine with probes had little or no effect on motility (see Methods). Results were confirmed by also attaching probes at C328 and, in some instances, C330. To simplify the interpretation of results, a kinesin monomer (K349) was used, because the two heads of a microtubule-bound kinesin dimer are thought to be in different conformational states[10–12].

## Mobility changes detected by EPR

We measured electron paramagnetic resonance (EPR) spectra derived from a paramagnetic probe attached to C333 (Fig. 2). We present our results in terms of a cycle in which soluble kinesin docks onto a microtubule, binds ATP, hydrolyses it and releases products.

In solution, the EPR spectra were superimposable in several nucleotide states (ADP, AMP-PNP, ADP-$AlF_4^-$ and ADP-$BeF_x$; last two not shown). The shape of the three sharp lines indicated that the probe was highly mobile, and behaved as if attached to a mobile protein loop[23]. When kinesin bound to the microtubule in the nucleotide-free state, the EPR spectrum was comparable to kinesin in solution; however, when AMP-PNP (a very slowly hydrolysed ATP analogue), ADP-$AlF_4^-$ or ADP-$BeF_x$ (data not shown) bound to microtubule-attached kinesin, a new spectral component appeared with peaks at high and low fields (Fig. 2). These spectra reveal a substantial decrease in mobility, which is indicative of a probe

attached to a rigid secondary structure element[23]. In the microtubule-bound ADP state, the EPR probe returned to a state of high mobility. Probes introduced at residues 328 and 330 produced results similar to those described above (data not shown), indicating that the spectral changes did not arise simply from altered local probe–protein interactions, but rather from a conformational change involving most of the neck linker.

Analysis of the temperature dependence of the spectra between 4 °C and 35 °C using the van't Hoff equation[24] showed that the change in enthalpy ($\Delta H$) for the transition to the AMP-PNP-induced conformation was −20, −15 and −8 kcal mol$^{-1}$ for residues 333, 330 and 328, respectively. Again, these large values indicate a significant protein conformational change, rather than an altered local probe–protein interaction; in addition, the variation of $\Delta H$ with position on the neck linker is consistent with a sequential zippering of the neck linker beginning at its N-terminal connection to the catalytic core. Collectively, our results indicate that the neck linker is mobile and becomes more ordered when the microtubule-bound motor binds an ATP analogue. After γ-phosphate release, the neck linker returns to its mobile conformation.

## Distance changes detected by FRET

To detect neck linker movements in different nucleotide states, fluorescence resonance energy transfer (FRET) was measured between dyes introduced at C333 and a nearby residue (C220) on the catalytic core (Fig. 1; Table 1). A nucleotide-dependent conformational change was not observed in solution, as the energy transfer efficiencies were similar with ADP or AMP-PNP (~85%). For kinesin bound to microtubules in the nucleotide-free state, the energy transfer efficiency was lower than in solution (76%). A significant increase in energy transfer (93%) was observed when microtubule-docked kinesin bound AMP-PNP, indicating that the two probes moved closer together by ~10 Å. We also measured FRET between residues 328 and 220, and obtained similar results to those described above (data not shown). Most of the AMP-PNP-induced motion must come from residue 333, as cryo-EM results (see below) indicate that residue 220 moves by less than 5 Å between the nucleotide-free and AMP-PNP states. The calculated distances between fluorescent probes (Table 1) and cryo-EM studies (see below) both suggest that the neck linker position most closely resembles the rat kinesin crystal structure in the microtubule-bound AMP-PNP state.

To probe the conformation of the neck linker without modifying its residues, we fused a green fluorescent protein (F64L, S65T GFP) to the C terminus of the neck linker at residue 339 (Fig. 1) and used it as a fluorescence donor for energy transfer to tetramethylrhodamine at C220. For microtubule-bound kinesin, FRET was higher in the AMP-PNP than in the nucleotide-free state (Fig. 3). Thus, GFP at the end of the neck linker moves closer to the tip of the catalytic core upon AMP-PNP binding, in agreement with the measurements described above.

We also examined FRET between C333 and C20, which is located at the opposite end of the catalytic core from 220 (Fig. 1). The change in FRET efficiency between nucleotide-free and AMP-PNP states on the microtubule (64.1 ± 6.3% and 42.3 ± 5.3% energy transfer, respectively) was opposite to that observed between C333 or K339–GFP and C220. Thus, in the nucleotide-free state, FRET reveals that the neck linker is positioned away from residue 220 and towards residue 20, which is most easily explained if it detaches from the catalytic core. In contrast, FRET between C20 and another catalytic core residue (C188) did not change significantly between nucleotide-free and AMP-PNP states on the microtubule (88.3 ± 3% and 87.0 ± 1.5% energy transfer, respectively).

In conclusion, FRET shows that the neck linker undergoes a large motion directed towards the tip of the catalytic core when microtubule-bound kinesin binds an ATP analogue. In contrast, for kinesin in solution, the FRET signal was nucleotide-independent and intermediate in value between the microtubule-bound

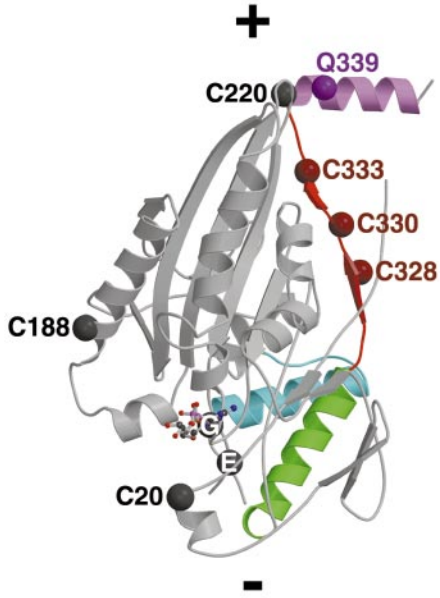


**Figure 1** Structure of the rat kinesin monomer[25] (numbered as in human kinesin). The kinesin structure is oriented as it docks onto the microtubule in Fig. 4 (+ and – indicate the direction of the microtubule plus and minus ends). The neck linker (residues 323–335) is red, the neck coiled-coil (336–349) is purple, α4 helix (256–270) and L12 (the microtubule binding loop; 270–281) are blue, and the α6 helix (residues 309–320) is green. ADP is shown in the active site as a ball-and-stick model. The mutated residues G234 and E236 near the nucleotide site are indicated by circles labelled 'G' and 'E'. Residue 339 marks the junction point in the K339–GFP fusion protein. Cysteines were introduced at positions 20, 188, 220, 328 and 333 (circles at Cα positions) for site-specific labelling in a 'cys-light' kinesin.

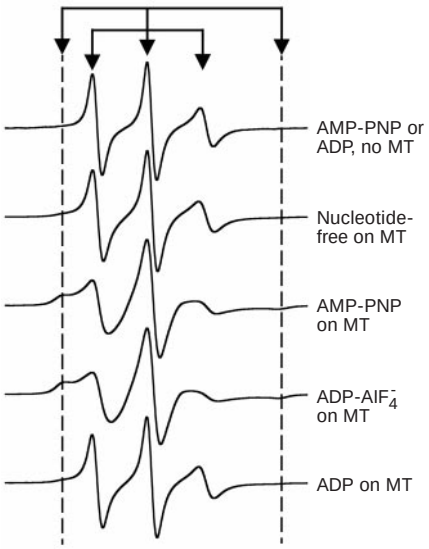


**Figure 2** Electron paramagnetic resonance spectra for kinesin C333–MSL in several nucleotide states, both free in solution and bound to microtubules. The two sets of resonance peaks are indicated by arrows. The narrower resonance peaks are indicative of a highly mobile probe, whereas the wider set of resonance peaks (highlighted by the vertical dashed lines) are indicative of restricted mobility and emerge in the triphosphate states on microtubules. This mobility shift can be modelled by a restriction in probe motion from a cone angle of ~120° to 32° (ref. 50).

nucleotide-free and AMP-PNP states, suggesting that the neck linker may exist in docked and mobile conformations. In support of this idea, solution scattering studies have shown that the kinesin dimer can adopt multiple configurations[27,28]. Furthermore, the neck linker is docked and disordered in the ADP crystal structures of rat[25,26] and human[3] kinesins, respectively. This suggests that the crystallization conditions for rat kinesin may have shifted a conformational equilibrium of the neck linker towards docking onto the catalytic core in its ADP state. Precedence for this exists in myosin, for which two markedly different crystal conformations were obtained with bound ADP-$BeF_x$[14,29], and an ADP structure has been reported to mimic an ATP configuration[30].

## Structural changes visualized by cryo-EM

We sought to visualize the position of the neck linker directly by cryo-EM (Fig. 4). As the 15-amino-acid neck linker is not visible in our electron image maps, we used a gold cluster attached to C333 as a reporter of its position. In the nucleotide-free state, two density peaks for the gold particle were observed: one lying towards the minus end (called the −30° position relative to the axis perpendicular to the microtubule), and the second lying towards the plus end (+125° position) (Fig. 4a). The occurrence of two peaks, when a single residue was labelled, indicates that the neck linker exists in an equilibrium between two positions that are similar in energy. Further support for this idea comes from the finding that the relative strengths of the +125° and −30° peaks vary among independent 3D maps of the nucleotide-free state (data not shown). The above results reveal that the neck linker can attach to the catalytic core in the nucleotide-free state, which would seem to contradict the high mobility measured in the EPR studies. However, EPR shows that the neck linker in nucleotide-free and ADP states becomes increasingly immobilized when cooled to 4 °C. Thus, the weak binding sites observed by cryo-EM may be populated during the freezing process.

For the motor–microtubule complex with AMP-PNP, the gold density was located at a third position, which is also near the tip of the catalytic core (+50° position) (Fig. 4b). This location also corresponds roughly to the position of the second head in the kinesin dimer in the microtubule-bound, AMP-PNP state[22]. A similar position (within 5 Å) was observed for the ADP-$AlF_4^-$ state (Fig. 4c). For both AMP-PNP and ADP-$AlF_4^-$, the occurrence of a single, strongly-diffracting peak suggested nearly 100% occupancy at this single position. Thus, after the motor binds AMP-PNP, the neck linker undergoes a marked transition from dual site occupancy at positions +125° and −30° to that of a single position at +50°.

**Table 1 FRET between donor (coumarin, CPM) and acceptor (tetramethylrhodamine, TMR) probes attached to the neck linker (C333) and the catalytic core (C220) in wild-type kinesin monomer and two ATP nonhydrolysing mutants**

| Kinesin (K349–C220, C333) | Nucleotide | MT | Energy transfer (%) |
|---|---|---|---|
| Wild type | ADP | – | 87.6 ± 3.3 |
| | AMP-PNP | – | 84.4 ± 0.2 |
| | Nucleotide-free | + | 76.4 ± 2.8 |
| | AMP-PNP | + | 93.4 ± 1.3 |
| G234A | ADP | – | 70.9 ± 6.1 |
| | Nucleotide-free | + | 70.1 ± 3.5 |
| | ATP | + | 75.1 ± 6.8 |
| | AMP-PNP | + | 78.4 ± 5.2 |
| E236A | ADP | – | 83.1 ± 4.5 |
| | Nucleotide-free | + | 69.9 ± 7.3 |
| | ATP | + | 95.1 ± 1.3 |
| | AMP-PNP | + | 92.3 ± 5.4 |

The mean and standard deviation are shown for at least three measurements. The maximum limiting anisotropy of the kinesin-bound probes did not change in the nucleotide-free and AMP-PNP states on microtubules (0.27 for CPM and 0.23 for TMR), indicating that the increase in energy transfer efficiency is due to a change in distance rather than a probe re-orientation. For wild type kinesin, the estimated probe–probe distances in the nucleotide-free and AMP-PNP states were about 34 Å and 24 Å, respectively. MT, microtubule; +, presence; –, absence of microtubules.

When the gold-labelled motor was bound to microtubules in the presence of 5 mM ADP, densities at the +125° and −30° positions were again observed (Fig. 4d). Similar results were obtained with a gold cluster attached to residue 328 (data not shown), indicating that most of the neck linker undergoes a similar nucleotide-dependent conformational change.

In contrast to the pronounced movements of the neck linker, the 3D maps of unlabelled K349 show only subtle differences between the AMP-PNP and nucleotide-free states (Fig. 4e). In addition, when the catalytic core was labelled at position 220, the gold density moved only slightly (<5 Å) between the nucleotide-free and AMP-PNP states (Fig. 4e, f). Thus, although small conformational changes may occur, the catalytic core does not shift its orientation on the microtubule upon nucleotide binding.

The orientation of the atomic structure in the cryo-EM maps must be established to determine how the neck linker is positioned in the catalytic core in its different nucleotide states; however, three different docking models have been reported[21,31–33]. To resolve this controversy, we labelled residues 20 and 188 simultaneously with gold particles (Fig. 4h). Residues 20, 188 and 220 form a triangle on the catalytic core, and the three gold positions allowed us to orient the crystal structure unambiguously in the electron microscopy maps (details will be reported elsewhere). Figure 1 shows the docking orientation of the kinesin crystal structure from the same view as Fig. 4. The results agree closely with our previous model[31], but not with other reported docking orientations[21,32]. In our docking of the catalytic core, the location of residue 333 in the kinesin crystal structure corresponds to the +50° gold position observed with ATP analogues (compare Figs 1 and 4). At atomic resolution, however, the microtubule-bound ATP state may not be identical to the crystal structure, which reveals relatively weak contacts between the neck linker and the catalytic core. It is possible that subtle rearrangements strengthen the neck linker–catalytic core interactions in the presence of microtubules and ATP analogues.

Thus, cryo-EM shows that the catalytic core maintains its overall position and orientation on the microtubule throughout the ATPase cycle. In contrast, the neck linker exhibits a striking

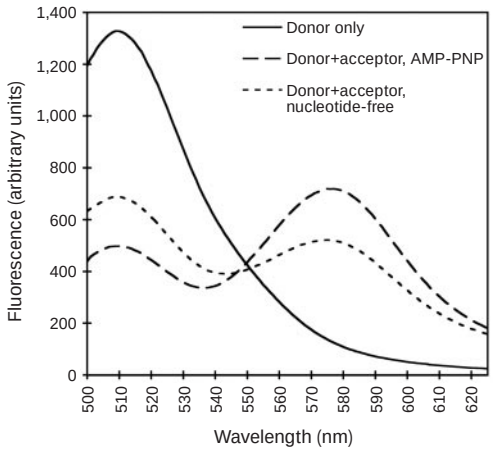


**Figure 3** Nucleotide-dependent energy transfer between GFP (donor) at the end of the neck linker and tetramethylrhodamine (acceptor) at C220. The emission spectrum of microtubule-bound K339–GFP without acceptor is shown by the solid black line; the spectrum was identical in 5 mM Mg-AMP-PNP and in the absence of nucleotide on microtubules (MT). In the presence of TMR acceptor at position 220, GFP fluorescence is quenched. There is significantly greater donor quenching (488 nm) and a corresponding enhancement of acceptor fluorescence (575 nm) in the presence of AMP-PNP than in the absence of nucleotide (energy transfer efficiencies of 60.6 ± 2.3% and 52.1 ± 5.1%, respectively). The difference in energy transfer was somewhat lower than with other fluorescent probes (Table 1), probably because GFP was somewhat mobile, even in the AMP-PNP state, as the result of its flexible connection to the kinesin neck linker.

nucleotide-dependent behaviour. In the absence of bound nucleotide, the neck linker is distributed between forward (+125°) and backward (−30°) pointing states that are separated by ~50 Å. On the basis of these two positions, we predict that the neck linker is able to pivot about a point that lies near the C terminus of α6. Subsequent binding of ATP analogues to the catalytic core locks the neck linker into a second forward pointing position at +50°. After phosphate release, however, the neck linker is again mobile and weakly interacts with two sites on the catalytic core.

### ATPase kinetics of G234A and E236A mutants

We identified two mutations in the switch II region (G234A and E236A; Fig. 1) which provided further insight into the kinesin mechanism. G234 in kinesin corresponds to conserved glycines in the active sites of G proteins and myosin, which form a hydrogen bond with the γ-phosphate and trigger a conformational change between the NTP and NDP states[4]. Kinesin E236 is positioned farther away and does not directly contact the nucleotide. Kinetic analysis of these mutants and conformational studies (see below) provide evidence that neck linker docking to the catalytic core is necessary for kinesin stepping.

The G234A and E236A mutants did not move microtubules in a gliding assay and had very low ATPase activities ($<0.04\ s^{-1}$ in the presence of microtubules). The second order rate constants for the binding of mant ATP (a fluorescent ATP analogue) to mutant and wild-type kinesins were the same ($\sim 2 \times 10^6\ M^{-1}\ s^{-1}$). Unlike wild-type kinesin, however, both mutants did not display a phosphate burst after [γ-$^{32}$P]ATP was added to nucleotide-free proteins (data not shown), indicating that the hydrolysis step is rate-limiting and more than 1,000-fold slower than in wild-type kinesin.

Although G234A and E236A were similarly defective in ATP hydrolysis, further kinetic studies suggested that E236A, but not G234A, can take a single ATP-induced step on the microtubule. A two-step process has been described[10–12] that leads to ADP release from a kinesin dimer, which reveals communication between the two heads. After rapid mixing with microtubules, one head releases its ADP rapidly ($100\ s^{-1}$; Table 2, reaction 2), whereas the second does so much more slowly ($\sim 0.4\ s^{-1}$)[11,12], indicating that it is constrained from interacting with the microtubule. ATP binding to the microtubule-bound head causes a conformational change that enables the detached partner head to step forward to the next tubulin binding site and release its ADP (Table 2, reaction 3). Both the G234A and E236A mutants in solution released mant ADP much faster than wild type, but microtubules further increased

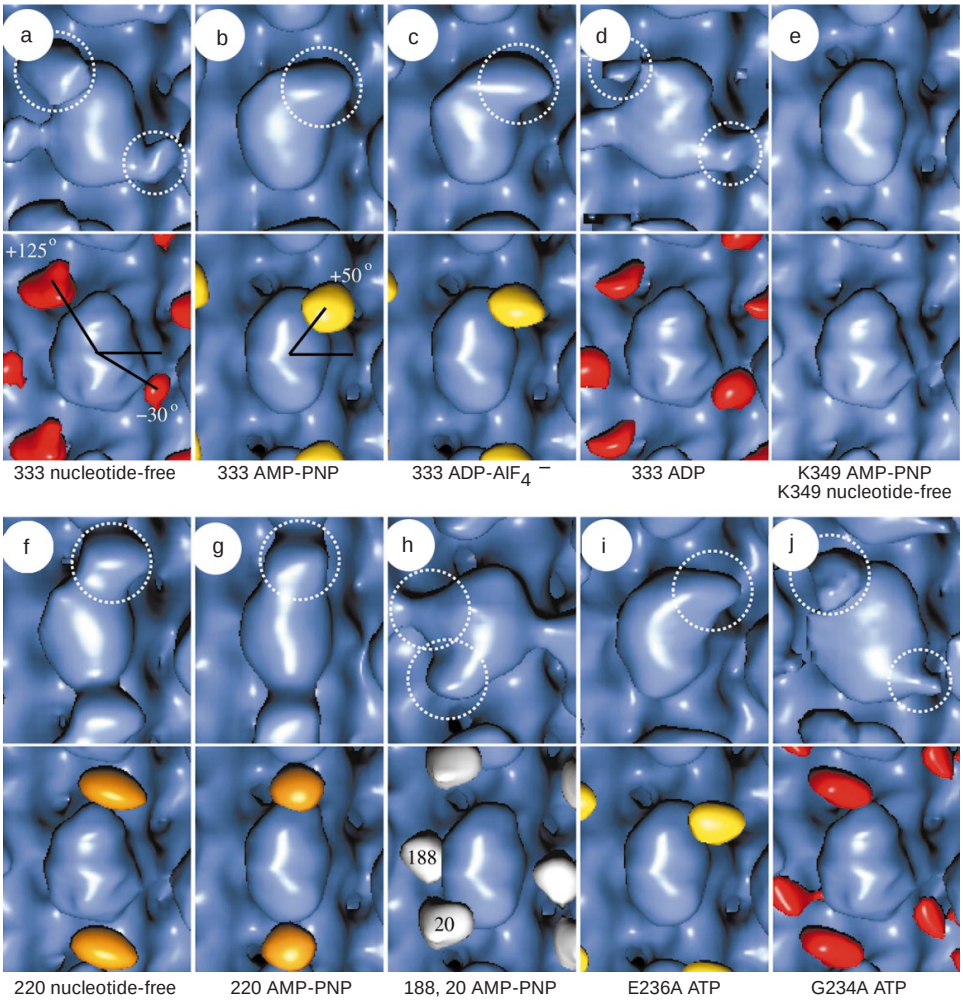


**Figure 4** Three-dimensional and difference maps of gold labelled motors attached to microtubules calculated by cryo-EM and image analysis. Unlabelled controls used in the difference mapping are shown in **e** (see Methods). Density associated with a single motor domain is centred in each panel; additional densities in the corners of some panels are from adjacent motors on the microtubule surface lattice. The microtubule protofilament to which the motor is attached runs vertically with the plus end at the top. Density attributable to the gold particle is identified by dotted circles in the raw 3D maps and is coloured in the difference maps. Difference maps are displayed with the control map that was used in the calculation. Red (**a**, **d**, **j**) and yellow (**b**, **c**, **i**) difference maps identify nucleotide states with ADP-like and ATP-like neck linker conformations respectively. Orange difference maps (**f**, **g**) show the position of the gold particle attached to residue 220 in two nucleotide states, which indicates that the catalytic core is immobile. The white difference map (**h**) shows gold particles attached to residues 20 and 188. The data in panels **g** and **h** confirm the docked orientation of the atomic model published earlier[31].

these rates (Table 2). For E236A, ATP also accelerated ADP release from the second head by more than 100-fold, to the rate observed for wild-type kinesin (Table 2). As E236A cannot hydrolyse ATP on this timescale, this result confirms speculations based upon nucleotide analogues[11,12] that ATP binding, and not a subsequent event in the cycle, causes the conformational change that leads to forward stepping. In contrast, ATP binding to the microtubule-bound G234A head caused only a 1.5-fold acceleration of ADP release by the second head, indicating a defect in head–head communication. Thus, our results show that E236A, but not G234A, can execute an ATP-binding-induced conformational change that allows the partner head to step to the next tubulin-binding site and release its ADP. These results also show interesting parallels with those obtained from two comparable ATP nonhydrolysing switch II mutations in *Dictyostelium* myosin (G457A and E459A), which are trapped in pre- and post-ATP 'power stroke' states, respectively[16].

## Neck linker docking in E236A but not G234A

If the ATP-driven conformational change in the neck linker is important for kinesin stepping, then ATP binding should be able to dock the neck linker onto the catalytic core in E236A, but not G234A. To test this hypothesis, we examined FRET between probes positioned at 220 and 333 in these two mutants. G234A showed no significant nucleotide- or microtubule-dependent changes in energy transfer efficiency; the values were comparable to that of nucleotide-free wild-type kinesin bound to microtubules (Table 1). However, a large FRET increase (a distance change of ~10 Å) was observed when microtubule-docked E236A bound either ATP or AMP-PNP. The comparable FRET signals obtained with ATP and AMP-PNP indicate that AMP-PNP mimics a normal nucleotide triphosphate state.

The neck linker conformations in the ATP state of the microtubule-bound G234A and E236A mutants were also examined by cryo-EM (Fig. 4). Consistent with the FRET results, the C333-attached gold particle on E236A-ATP was located at the +50° position at the tip of the catalytic core, similar to wild-type kinesin with AMP-PNP (Fig. 4h). For G234A-ATP, however, weak gold particle densities were detected at the +125° and −30° positions, but not at +50°, which is similar to that observed for wild-type kinesin in the nucleotide-free and ADP states (Fig. 4g).

In conclusion, for E236A bound to microtubules, the neck linker is displaced from the tip of the catalytic core in the absence of nucleotide and redocks after ATP binding. Thus, E236A undergoes both ATP-induced neck linker docking and motor stepping to elicit ADP release (Tables 1, 2). In contrast, even with ATP in the active site, the neck linker of G234A is in an ADP-like state, and it cannot advance its partner head effectively to the next subunit. The G234A result also reveals that hydrogen bonding of switch II to the γ-phosphate is necessary for triggering ATP-induced neck linker docking.

**Table 2 Release of mant ADP from wild-type and mutant kinesin dimers (K420)**

| Reaction | 1 | 2 | 3 |
|---|---|---|---|
| | 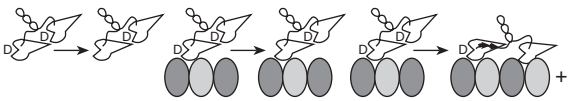 | | |
| Protein | | | |
| Wild type | 0.01 ± 0.002 (1) | 100 ± 10 (10,000) | 120 ± 20 (12,000) |
| G234A | 10 ± 1 (1) | 40 ± 10 (4) | 15 ± 3 (1.5) |
| E236A | 1.1 ± 0.3 (1) | 100 ± 15 (91) | 120 ± 17 (109) |

To determine the rate constant for reaction 1, K420-mant ADP (3 μM site concentration) was reacted with 500 μM ATP. For reaction 2, K420-mant ADP was reacted with a range of microtubule concentrations; the maximal rates are reported here. The amplitude of the fluorescence signal was roughly half that observed in the presence of ATP. For reaction 3, the K420-mant ADP was first mixed with 10–20 μM microtubules, and the one-head bound intermediate was then reacted with 500 μM ATP to promote the release of the remaining mant ADP.
* Fold rate increase compared with reaction 1 is given in parentheses.

## The kinesin force-generating cycle

Cryo-EM, EPR and FRET studies have provided complementary information for understanding how the neck linker changes its structure during kinesin's enzymatic cycle. Beginning a cycle with kinesin-ADP in solution, EPR and FRET suggest that the neck linker is not rigidly attached to the catalytic core. After kinesin binds to the microtubule and releases its ADP the neck linker is primarily detached, but, upon ATP binding, the neck linker rigidly docks onto the catalytic core in a single position (+50°) that agrees with that seen in the crystal structure. This conformational change requires both microtubules and a γ-phosphate in the active site, as it is only observed with ATP, AMP-PNP and ADP-$AlF_4^-$. The last result also suggests that the docked state may be maintained in the ADP-$P_i$ state in the normal enzymatic cycle. After phosphate release, the neck linker reverts to its more mobile conformation, and the

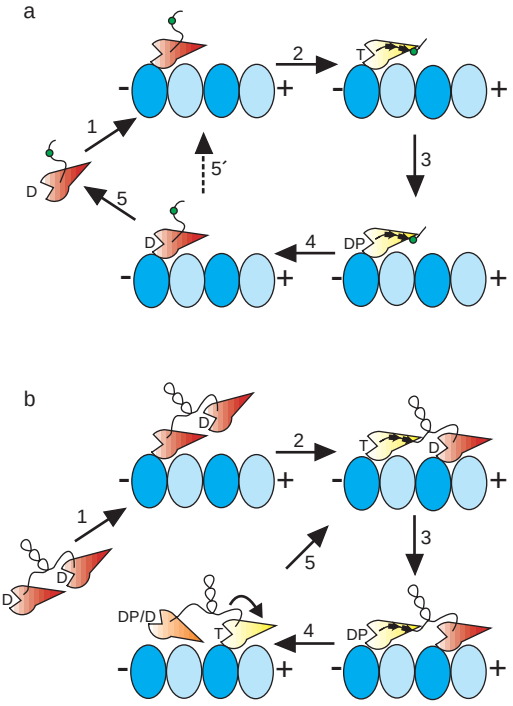


**Figure 5** Models for motility by truncated kinesin monomers and processive dimers. Microtubule-bound, nucleotide triphosphate states are shown in yellow, and other states in red. The α- and β-subunits of tubulin are shown in two shades of blue. **a**, Kinesin monomers. Once bound to the microtubule, ATP (T) binding causes the neck linker to dock onto the catalytic core (step 2), which causes movement of position 333 (green circle) towards the microtubule plus end. Previous work has shown that, in solution, the monomer-ADP (D) state may not dissociate during each ATPase cycle[37,38] (step 5′). This would reduce the velocity of motion; however, strain created by several active kinesin motors attached to the same microtubule may promote monomer-ADP detachment, leading to more efficient movement[9,37,38] (step 5). **b**, Processive dimers. In the dimer cycle, one head initially attaches to the microtubule, releasing its ADP (step 1). ATP binding to this head causes neck linker docking and displacement of the partner head to a forward binding site (step 2). ATP is exchanged for ADP in the forward head (steps 3 and 4) causing the re-zippering of the neck linker. Detachment of the rear head (in either an ADP-$P_i$ (DP) or ADP state) may be aided either by this re-zippering (as shown) or earlier by the weak to strong microtubule binding transition in the forward head. Once detached, the rear head would reattach to a forward binding site 16 nm away because of completed neck linker docking by the partner head (step 5). For kinesin walking down the microtubule, the cycle would continue through the three states shown (3, 4 and 5), and both heads would be microtubule bound for most of the time.

motor binds more weakly to the microtubule[34]. The above model is likely to apply to dimeric kinesin, although the neck coiled-coil and head–head contacts[26] may affect the conformation of the detached neck linker.

A model for how ATP-induced neck linker docking can drive kinesin motility is shown in Fig. 5. Kinesin binds to the microtubule with its catalytic core tip pointing towards the microtubule plus end (Figs 1 and 4). For the kinesin monomer (Fig. 5a), the docking of the neck linker from its various nucleotide-free positions to its single ATP position on the catalytic core would cause a plus-end-directed displacement. EPR results suggest that this transition might occur by a sequential zippering of the neck linker that begins at α6 and ends at the tip of the catalytic core. In this model, force generation does not occur by a 'power stroke' between two well-ordered states, as is generally described for myosin. Instead, movement involves a transition from a disordered to an ordered state, with ATP binding providing the energy source for rectifying this Brownian ratchet. This model also predicts that force generation in the monomer occurs upon ATP binding[35] and that multiple monomers, each producing small displacements, must interact simultaneously with a microtubule to produce movement[7,9] (Fig. 5).

Neck linker movements could also explain processive motion by the kinesin dimer (Fig. 5b). Neck linker docking induced by ATP in the microtubule-bound head would position the partner head closer to the microtubule plus end[22]. Even if the neck coiled-coil remains intact, the partner head can then attach to the forward tubulin subunit[36]. Once the two-head-bound intermediate is formed, ADP/ATP exchange in the forward head again triggers zippering of the neck linker, and this process could assist in dissociating the rear head[9,37,38] and displacing it by 16 nm to the next available forward binding site. The net result of this action would be a rapid 8-nm step[6]. The bias for plus-end-directed motion in the kinesin dimer is generated through both neck linker docking and microtubule binding by the forward head. In this model, neck linker movement provides the trigger that allows motor stepping, although changes in the neck coiled-coil or in head–head interactions may augment this process[33,36]. The model also suggests that a backward load could slow down the motor[39] by decreasing the rate of neck linker docking and cause kinesin to take a backward step at stall loads[40] by reversing this process. A forward load could speed up movement[40] by favouring neck linker docking and/or by accelerating the dissociation of the rear head.

## Comparison with other motors

The motility-producing conformational change described here for kinesin differs significantly from the rotation of myosin's rigid lever arm which is triggered by phosphate release[13,14,30]. In both motors, however, the communication mechanism from the active site to the mechanical element probably operates through structurally and functionally analogous nucleotide-binding loops and helices[3] (for example, switch II, α4 and α6; Fig. 1). In addition, the neck linker of kinesin emerges from the catalytic core in a similar position to the reactive-sulphydryl helix of myosin[3], which is also thought to undergo a disordered-to-ordered transition during the ATPase cycle of myosin[30,41]. Myosin's reactive sulphydryl helix is believed to be essential for driving a 'rearward-to-forward' motion of the converter-lever arm complex, similar to the rearward-to-forward movement of the partner kinesin head triggered by the neck linker. Thus, although differently engineered, the converter–lever-arm complex of myosin, and the second head–neck coiled-coil of kinesin may be analogous structures that respond to a similarly positioned 'trigger' peptide.

Our proposed kinesin mechanism also reveals similarities to other mechanically active enzymes. Kinesin's motility-producing conformational change is driven by ATP binding, but this nucleotide-dependent conformational change requires motor contact with its microtubule substrate. Similarly, in $F_1$-ATP synthase[42,43] and GroEL[44], functionally relevant conformational changes are driven by ATP binding while these enzymes are complexed with their partner proteins (the γ subunit for $F_1$ and GroES for GroEL). A simultaneous requirement of ATP and the partner protein for triggering a conformational change ensures tight coupling between ATP-binding energy and mechanical work in all of these enzymes. □

## Methods

### Cloning and protein purification

Solvent-exposed cysteines were mutated to Ser/Ala (C7S, C65A, C168A, C174S, C294A, C330S and C421A) by QuikChange mutagenesis (Stratagene) of a human K560–$His_6$ construct in a pET17b vector[17]. Buried cysteines at positions 13, 301 and 302 were retained. This 'cys-light' kinesin was unreactive to thiol-reactive agents, exhibited normal microtubule gliding velocity (cys-light K560 and wild-type K560: 19.3 ± 2.8 and 20.2 ± 3.6 μm $min^{-1}$, respectively) and microtubule-stimulated ATPase activity (cys-light K560 and wild-type K560: catalytic rate constant ($k_{cat}$) − 19.3 ± 1.5 and 28.6 ± 4.2 ATP $head^{-1}$ $s^{-1}$, respectively; Michaelis constant ($K_m$)MT − 1.2 ± 0.5 and 1.2 ± 0.6 μM tubulin, respectively), and moved processively as determined using a single molecule fluorescence assay[17]. Other constructs described in this study were prepared using QuickChange mutagenesis and/or PCR subcloning and were confirmed by DNA sequencing.

Proteins were expressed in BL21(DE3)[17], and K560[17], K420[27] and kinesin–GFP fusion proteins[17] were purified as previously described. Purification of cys-light K349 was done as described[45], except that HEPES buffer was used instead of PIPES, and a final RESource Q column was run at pH 8 with 0.5 mM Tris-carboxyethyl phosphine-HCl (TCEP) instead of dithiothreitol. Proteins were frozen in 20% w/v sucrose and stored in liquid nitrogen.

### Enzymology and motility assays

Steady-state, microtubule-stimulated ATPase rates were measured using a coupled enzymatic assay[46] or by hydrolysis of [γ-$^{32}$P]ATP[34]. Dissociation kinetics of mant ADP from kinesin was done as described[34] in 25 mM PIPES, pH 6.9, 2 mM $MgCl_2$, 1 mM EGTA and 50 mM NaCl.

Tubulin preparation and microtubule gliding assays for K560 proteins were done as described[46]. Monomer motility was measured in K339–GFP using anti-GFP antibodies to attach the protein to the surface[17]. The motility was assayed in FRET labelling buffer (see below) with 0.5 mM TCEP-HCl, 2 mg $ml^{-1}$ casein, 10 μg $ml^{-1}$ unlabelled microtubules, 20 μM taxol, an oxygen depleting system and 1 mM ATP; microtubules were visualized using DIC microscopy, and more than 25 velocity measurements were made. For testing the motility of chemically modified kinesins, probes were labelled to ~100% stoichiometry as confirmed by mass spectroscopy, fluorescence or gel-shift assays. The microtubule gliding velocities produced by MSL–C333 K339–GFP, TMR/CPM–C220/C333 K339–GFP, TMR–C220 K339–GFP and undecagold-C333 K339–GFP were 107.8%, 81.9%, 98.9% and 86.6% of the cys-light K339–GFP control, which moved at 2.4 μm $min^{-1}$.

### Chemical modification of kinesin

For EPR, a single cysteine-containing kinesin in EPR labelling buffer (25 mM PIPES, pH 7, 50 mM NaCl, 2 mM $MgCl_2$, 1 mM EGTA and 10 μM ATP) was incubated with a 2–5-fold molar excess of 4-maleimido-2,2,6,6-tetramethyl-1-piperidinoxy (MSL; Sigma) overnight at 4 °C. Excess spin label was removed as described[24]. The labelling stoichiometry was determined by measuring protein concentration (Bradford assay with BSA standards) and probe concentration (by comparing labelled protein to known concentrations of MSL[24]).

For FRET, double-cysteine containing kinesin (K349) was dialysed against FRET labelling buffer (EPR buffer at pH 7.5 with 0.1 mM TCEP) and reacted with 7-diethylamino-3-(4′-maleimidylphenyl)-4-methylcoumarin (CPM, Molecular Probes) for 3 h at room temperature at a stoichiometry of ~1 dye per 10 reactive cysteines. Half of the CPM-labelled kinesin (or K339–GFP) was removed (donor-labelled kinesin), and the remainder (donor–acceptor-labelled kinesin) was incubated for 3 h at room temperature with a 10-fold excess of tetramethylrhodamine-6-maleimide to cysteines (TMR, Molecular Probes) which reacted with the remaining reactive sites. Thus, almost all donor-labelled kinesins were modified with an acceptor probe. Removal of free dye was done as described[24]. The labelling stoichiometry was determined by measuring dye absorbance and protein concentration[46].

For gold-cluster labelling, monomaleimide-undecagold labelling was carried out for 16 h at 4–5-fold excess[47]. Unbound gold-cluster and aggregated material were removed by ion exchange and gel filtration chromatography. Undecagold labelling shifted the mobility of kinesin in non-denaturing PAGE; the extent of labelling assessed by this method was 80–100%.

### Spectroscopy

Electron-paramagnetic resonance spectra were obtained, and the $\Delta H$ was determined as described[24]. For EPR, kinesin was incubated with either 5 mM Mg-AMP-PNP, 5 mM Mg-ADP, 2 mM Mg-ADP-$AlF_4^-$ (2 mM $AlCl_3$, 10 mM KF), or apyrase (6.6 U $ml^{-1}$) (nucleotide-free). In solution, 50–80 μM kinesin was used. For kinesin-microtubule samples, 25–30 μM kinesin was mixed with 125–150 μM polymerized tubulin, the complex centrifuged, and microtubule pellet analysed to ensure that essentially all kinesin was bound to microtubules.

Fluorescence resonance energy transfer samples contained ~1 μM kinesin (in FRET labelling buffer), ±10 μM microtubules, 5 mM of the indicated magnesium nucleotide or 25 U ml$^{-1}$ apyrase to generate the nucleotide-free state. The microtubule-bound, ADP state and the solution, nucleotide-free state could not be measured because of excessive light scattering from high microtubule concentrations and protein denaturation, respectively. Using a K2 spectrofluorimeter (ISS), fluorescence was measured at two serial twofold dilutions to ensure that energy transfer was not dilution sensitive because of inner filter effects or reabsorption of donor emission. GFP and CPM were excited at 475 nm and 395 nm respectively, and TMR emission was measured at 575 nm. Energy transfer to the nearby acceptor was measured by the reduction in donor fluorescence ($E = 1 - (Fl_{DA}/Fl_{DO})$, where $Fl_{DO}$ and $Fl_{DA}$ are the donor fluorescence in the absence and presence of the acceptor, respectively[48]). Energy transfer for K339–GFP–TMR samples was calculated both by donor quenching and acceptor enhancement[48]; both methods yielded similar values. Donor–acceptor distance was calculated from Förster's equation, assuming orientation parameter $\kappa^2$ to be two-thirds (ref. 49), a quantum yield of 0.5 for coumarin[48], and a spectral overlap for coumarin-tetramethylrhodamin of $6.4 \times 10^{14}$ M$^{-1}$ cm$^{-1}$ nm$^4$ (ref. 48).

### Cryo-EM and image analysis

Frozen grids of decorated microtubules were prepared and imaged as described[31] with some modifications. Microtubule decoration with gold-labelled kinesin heads (2–10 mg ml$^{-1}$) was carried out in 80 mM PIPES (pH 6.8), 1 mM $MgCl_2$, 1 mM EGTA supplemented with 5 mM magnesium nucleotide or apyrase (100–200 U ml$^{-1}$) (nucleotide-free). Images of helical 15-protofilament microtubules were analysed as described[31]. Two unlabelled control maps (K349 with AMP-PNP and nucleotide-free K349) were used for difference mapping. Subtle structural features of the core regions of the raw gold labelled 3D maps dictated which control map was used for the difference calculation. Thus, difference maps of nucleotide-free and ADP-containing complexes and of G234A with ATP were calculated using the nucleotide-free control map. The remaining difference maps were calculated using the K349-AMP-PNP control map. The number of data sets averaged and the total number of molecules for each of the raw 3D maps shown in Fig. 4 were 22 data sets, 10,780 molecules (a); 42, 21, 280 (b); 18, 7420 (c); 25, 16,380 (d); 28, 18,620 (e, top); 28, 12,460 (e, bottom); 14, 6,160 (f); 18, 10,360 (g); 16, 7,980 (h); 11, 10,500 (i); and 18, 6,440 (j).

Received 9 September; accepted 11 November 1999.


1. Goldstein, L. S. B. & Philp, A. V. The road less traveled: emerging principles of kinesin motor utilization. *Annu. Rev. Cell Dev. Biol.* **15,** 141–183 (1999).
2. Vale, R. D. & Fletterick, R. J. The design plan of kinesin motors. *Annu. Rev. Cell Dev. Biol.* **13,** 745–777 (1997).
3. Kull, F. J., Sablin, E. P., Lau, R., Fletterick, R. J. & Vale, R. D. Crystal structure of the kinesin motor domain reveals a structural similarity to myosin. *Nature* **380,** 550–555 (1996).
4. Sablin, E. P., Kull, F. J., Cooke, R., Vale, R. D. & Fletterick, R. J. Crystal structure of the motor domain of the kinesin-related motor ncd. *Nature* **380,** 555–559 (1996).
5. Howard, J., Hudspeth, A. J. & Vale, R. D. Movement of microtubules by single kinesin molecules. *Nature* **342,** 154–158 (1989).
6. Svoboda, K., Schmidt, C. F., Schnapp, B. J. & Block, S. M. Direct observation of kinesin stepping by optical trapping interferometry. *Nature* **365,** 721–727 (1993).
7. Berliner, E., Young, E. C., Anderson, K., Mahtani, H. & Gelles, J. Failure of a single-headed kinesin to track parallel to microtubule protofilaments. *Nature* **373,** 718–721 (1995).
8. Vale, R. D. *et al.* Direct observation of single kinesin molecules moving along microtubules. *Nature* **380,** 451–453 (1996).
9. Hancock, W. O. & Howard, J. Processivity of the motor protein kinesin requires two heads. *J. Cell Biol.* **140,** 1395–1405 (1998).
10. Hackney, D. D. Evidence for alternating head catalysis by kinesin during microtubule-stimulated ATP hydrolysis. *Proc. Natl Acad. Sci. USA* **91,** 6865–6869 (1994).
11. Ma, Y.-Z. & Taylor, E. W. Interacting head mechanism of microtubule-kinesin ATPase. *J. Biol. Chem.* **272,** 724–730 (1997).
12. Gilbert, S. P., Moyer, M. L. & Johnson, K. A. Alternating site mechanism of the kinesin ATPase. *Biochemistry* **37,** 792–799 (1998).
13. Rayment, I. *et al.* Structure of the actin–myosin complex and its implications for muscle contraction. *Science* **261,** 58–65 (1993).
14. Dominguez, R., Freyzon, Y., Trybus, K. M. & Cohen, C. Crystal structure of a vertebrate smooth muscle myosin motor domain and its complex with the essential light chain: visualization of the pre-power stroke state. *Cell* **94,** 559–571 (1998).
15. Corrie, J. E. T. *et al.* Dynamic measurements of myosin light-chain-domain tilt and twist in muscle contraction. *Nature* **400,** 425–430 (1999).
16. Suzuki, Y., Yasunaga, T., Ohkura, R., Wakabayashi, T. & Sutoh, K. Swing of the lever arm of a myosin motor at the isomerization and phosphate-release steps. *Nature* **396,** 380–383 (1998).
17. Case, R. B., Pierce, D. W., Hom-Booher, N., Hart, C. L. & Vale, R. D. The directional preference of kinesin motors is specified by an element outside of the motor catalytic domain. *Cell* **90,** 959–966 (1997).
18. Henningsen, U. & Schliwa, M. Reversal in the direction of movement of a molecular motor. *Nature* **389,** 93–96 (1997).
19. Endow, S. A. & Waligora, K. W. Determinants of kinesin motor polarity. *Science* **281,** 1200–1202 (1998).
20. Arnal, I. & Wade, R. H. Nucleotide-dependent conformation of the kinesin dimer interacting with microtubules. *Structure* **1998,** 33–38 (1998).
21. Hirose, K., Lowe, J., Alonso, M., Cross, R. A. & Amos, L. A. Congruent docking of dimeric kinesin and ncd into three-dimensional electron cryomicroscopy maps of microtubule-motor ADP complexes. *Mol. Biol. Cell* **10,** 2063–2074 (1999).
22. Hirose, K., Lockhart, A., Cross, R. A. & Amos, L. A. Three-dimensional cryoelectron microscopy of dimeric kinesin and ncd motor domains on microtubules. *Proc. Natl Acad. Sci. USA* **93,** 9539–9544 (1996).
23. Mchaourab, H. S., Lietzow, M. A., Hideg, K. & Hubbell, W. L. Motion of spin-labeled side chains in T4 lysozyme. Correlation with protein structure and dynamics. *Biochemistry* **35,** 7692–7704 (1996).
24. Naber, N., Cooke, R. & Pate, E. Binding of ncd to microtubules induces a conformational change near the junction of the motor domain with the neck. *Biochemistry* **36,** 9681–9689 (1997).
25. Sack, S. *et al.* X-ray structure of motor and neck domains from rat brain kinesin. *Biochemistry* **36,** 16155–16165 (1997).
26. Kozielski, F. *et al.* The crystal structure of dimeric kinesin and implications for microtubule-dependent motility. *Cell* **91,** 985–994 (1997).
27. Stone, D. B., Hjelm, R. P. Jr & Mendelson, R. A. Solution structures of dimeric kinesin and Ncd motors. *Biochemistry* **38,** 4938–4947 (1999).
28. Marx, A. *et al.* Conformations of kinesin: solution versus crystal structures and interactions with microtubules. *Eur. Biophys. J.* **27,** 455–465 (1998).
29. Fisher, A. J. *et al.* X-ray structures of the myosin motor domain of *Dictyostelium discoideum* complexed with MgADP.BeFx and MgADP.$AlF_4^-$. *Biochemistry* **34,** 8960–8972 (1995).
30. Houdusse, A., Kalabokis, V. N., Himmel, D., Szent-Gyorgyi, A. G. & Cohen, C. Atomic structure of scallop myosin subfragment S1 complexed with MgADP: a novel conformation of the myosin head. *Cell* **97,** 459–470 (1999).
31. Sosa, H. *et al.* A model for the microtubule-ncd motor protein complex obtained by cryo-electron microscopy and image analysis. *Cell* **90,** 217–224 (1997).
32. Kozielski, F., Arnal, I. & Wade, R. H. A model of the microtubule-kinesin complex based upon electron cryomicroscopy and X-ray crystallography. *Curr. Biol.* **8,** 191–198 (1998).
33. Hoenger, A. *et al.* Image reconstructions of microtubules decorated with monomeric and dimeric kinesins: comparison with X-ray crystallography. *Curr. Biol.* **8,** 191–198 (1998).
34. Ma, Y. Z. & Taylor, E. W. Mechanism of microtubule kinesin ATPase. *Biochemistry* **34,** 13242–13251 (1995).
35. Romberg, L. & Vale, R. D. Chemomechanical cycle of kinesin differs from that of myosin. *Nature* **361,** 168–170 (1993).
36. Romberg, L., Pierce, D. W. & Vale, R. D. Role of the kinesin neck region in processive microtubule-based motility. *J. Cell. Biol.* **140,** 1407–1416 (1998).
37. Jiang, W. & Hackney, D. D. Monomeric kinesin head domains hydrolyze multiple ATP molecules before release from a microtubule. *J. Biol. Chem.* **272,** 5616–5621 (1997).
38. Moyer, M. L., Gilbert, S. P. & Johnson, K. A. Pathway of ATP hydrolysis by monomeric and dimeric kinesin. *Biochemistry* **37,** 800–813 (1998).
39. Visscher, K., Schnitzer, M. J. & Block, S. M. Single kinesin molecules studied with a molecular force clamp. *Nature* **400,** 184–189 (1999).
40. Coppin, C. M., Pierce, D. W., Hsu, L. & Vale, R. D. The load dependence of kinesin's mechanical cycle. *Proc. Natl Acad. Sci. USA* **94,** 8539–8544 (1997).
41. Thomas, D. D., Ramachandran, S., Roopnarine, O., Hayden, D. W. & Ostap, E. M. The mechanism of force generation in myosin: a disordered-to-order transition, coupled to internal structural changes. *Biophys. J.* **68** (suppl.), 135s–141s (1995).
42. Wang, H. & Oster, G. Energy transduction in the F1 motor of the ATP synthase. *Nature* **396,** 279–282 (1998).
43. Al-Shawi, M. & Nakamoto, R. Mechanism of energy coupling in the FoF1-ATP synthase: the uncoupling mutant, γM23K, disrupts the use of binding energy to drive catalysis. *Biochemistry* **36,** 12954–12960 (1997).
44. Weissman, J. S., Rye, H. S., Fenton, W. A., Beechem, J. M. & Horwich, A. L. Characterization of the active intermediate of a GroEL–GroES-mediated protein folding reaction. *Cell* **84,** 481–490 (1996).
45. Fujiwara, S., Kull, F. J., Sablin, E. P., Stone, D. B. & Mendelson, R. A. The shapes of the motor domains of two oppositely directed microtubule motors, ncd and kinesin: a neutron scattering study. *Biophys. J.* **69,** 1563–1568 (1995).
46. Woehlke, G. *et al.* Microtubule interaction site of the kinesin motor. *Cell* **90**, 207–216 (1997).
47. Safer, D. Undecagold cluster labeling of proteins at reactive cystein residues. *J. Struct. Biol.* **127,** 371–374 (1999).
48. Van Der Meer, B. W., Coker, G. & Chen, S.-Y. S. *Resonance Energy Transfer: Theory and Data* (VCH, New York, 1994).
49. dos Remedios, C. G. & Moens, P. D. Fluorescence resonance energy transfer spectroscopy is a reliable "ruler" for measuring structural changes in proteins. Dispelling the problem of the unknown orientation factor. *J. Struct. Biol.* **115,** 175–185 (1995).
50. Barnett, V. A., Fajer, P., Polnaszek, C. F. & Thomas, D. D. High resolution detection of muscle crossbridge orientation by EPR. *Biophys. J.* **49,** 144–147 (1986).


### Acknowledgements

We thank L. Sweeney for encouragement; A. Ruby for assistance with protein preparations; B. Sheehan for computing and image processing; and M. Tomishige for examining the processivity of cys-light K560–GFP. We thank R. Case and K. Thorn for comments on the manuscript. This work was supported, in part, by grants for the NIH (R.A.M., E.W.T., R.C. and R.D.V.), and the NSF (B.O.C.). S.R. is supported by the UCSF Graduate Group in Biophysics.

Correspondence and requests for materials should be addressed to R.D.V. (e-mail: vale@phy.uscf.edu).